

# Characterization of IIP2 and DC-Offsets in Transconductance Mixers

Kalle Kivekäs, *Student Member, IEEE*, Aarno Pärssinen, *Member, IEEE*, and Kari A. I. Halonen

**Abstract**—Envelope distortion in transconductance mixers is analyzed in this paper. The analysis consists of a simplified theoretical study, simulation results, and measurements about several implemented mixers. The studied mixers are active single-balanced and double-balanced structures. A theoretical mismatch analysis is carried out instead of a complex mixer nonlinearity analysis; this gives an intuitive sense of even-order nonlinearity in balanced mixers, and provides information about the fundamental restrictions of second-order input intercept point (IIP2) and the relations of different imbalances to actual performance. The analysis uses a number of simplifying assumptions, but without losing generality. The IIP2 is sensitive to any mismatch in a differential circuit topology. It will be shown that an excellent IIP2 can be achieved in slightly imbalanced conditions by a controllable mismatch device.

**Index Terms**—BiCMOS analog integrated circuits, DC offset, direct conversion, envelope distortion, IIP2, mismatch, mixers, nonlinearity, radio receivers, second-order distortion.

## I. INTRODUCTION

RECENT advances in silicon technologies have established a large variety of new opportunities to develop portable electronic equipment for wireless communications. The objective is to miniaturize devices without deteriorating their performance and to improve the cost effectiveness of the equipment. The direct conversion architecture has shown its capability in the integration of the radio receiver. However, it exhibits not only benefits, but also some disadvantages compared to superheterodyne receiver [1], [2]. One of the most limiting problems in the direct conversion receiver is the envelope distortion due to the even-order nonlinearities. Many cellular systems require an excellent second-order input intercept point (IIP2) performance if a direct conversion receiver architecture is used. Guidelines to estimate the specification for radio systems are discussed, e.g., in [3].

Intermodulation distortion [4]–[6] and noise performance [7]–[9] of current-commutating mixers have been analyzed quite extensively in the literature. However, the distortion analysis usually concentrates only on the odd-order nonlin-

earity. Few recent works have focused on the analysis of second-order distortion and, in particular, circuit techniques to reduce envelope distortion [3], [10]–[12]. In direct conversion, the second-order distortion adds another dimension to the conventional analysis because the performance is limited both by the circuit nonlinearities and symmetry. Hence, the envelope distortion analysis in the balanced circuits is not as straightforward as the analysis of odd-order nonlinear characteristics because the distortion at the output is a complex function of different mismatches in the circuit [13]. The interface of a mixer to the preceding stage, which is typically a low-noise amplifier (LNA) or a bandpass filter as in Fig. 1(a), is usually ac coupled and, thus, the second-order distortion due to the LNA is filtered out. Therefore, the most dominant second-order distortion source in a receiver is the downconversion stage. The mixers used in integrated direct conversion receivers are usually active transconductance mixers and practically always balanced- or double-balanced structures. Also, the transconductance stage is sometimes ac-coupled to the mixing core as in Fig. 1(b). Then, the second-order beat around dc generated in the transconductance stage is filtered out [2], [14]. However, this technique has not improved the performance of the mixer to the desired level and results are comparable to the other existing topologies. In a perfectly balanced case, the IIP2 is infinite and the result is independent of any other parameter as long as the balance is not violated.

This paper describes the analysis of envelope distortion in mixers by means of IIP2. Section II presents a theoretical mismatch analysis describing the basic behavior of the second-order distortion. Section III deals with the simulation results for corresponding mixer topologies as analyzed in Section II. Section IV gives the measured results of implemented circuits, and Section V summarizes the work.

## II. MISMATCH MODEL FOR SINGLE- AND DOUBLE-BALANCED MIXERS

The behavioral model of a single-balanced mixer is shown in Fig. 2(a). Its frequency conversion characteristics as well as the second-order nonlinearity performance will be illustrated by derived expressions. The transconductance stage is simply modeled with a voltage-controlled current source (VCCS) and the mixing transistors with ideal switches. The model is later extended to a double-balanced configuration, in Fig. 2(b). The dominant nonlinearity source in the transconductance mixer is assumed to be the input  $g_m$ -stage. This is not generally valid but we can assume that all significant nonlinearities can be referred

Manuscript received May 16, 2001; revised October 15, 2001. This work was supported by grants from Nokia Networks, Nokia Mobile Phones, Nokia Foundation, and the Finnish National Technology Agency (TEKES). This paper was recommended by Associate Editor H. Luong.

K. Kivekäs and K. A. I. Halonen are with the Electronic Circuit Design Laboratory, Department of Electrical and Communications Engineering, Helsinki University of Technology, FIN-02015, Helsinki, Finland (e-mail: kks@ecdl.hut.fi).

A. Pärssinen is with the Nokia Research Center, FIN-00180 Helsinki, Finland.

Publisher Item Identifier S 1057-7130(01)11307-8.

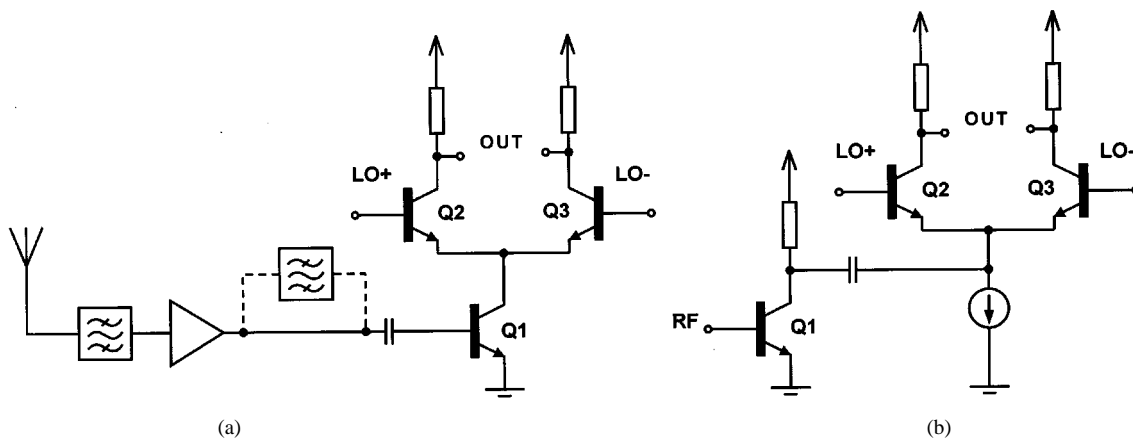


Fig. 1. (a) Single-balanced transconductance mixer and preceding RF parts. Sometimes a bandpass filter is required between LNA and mixer. (b) AC-coupled transconductance mixer.

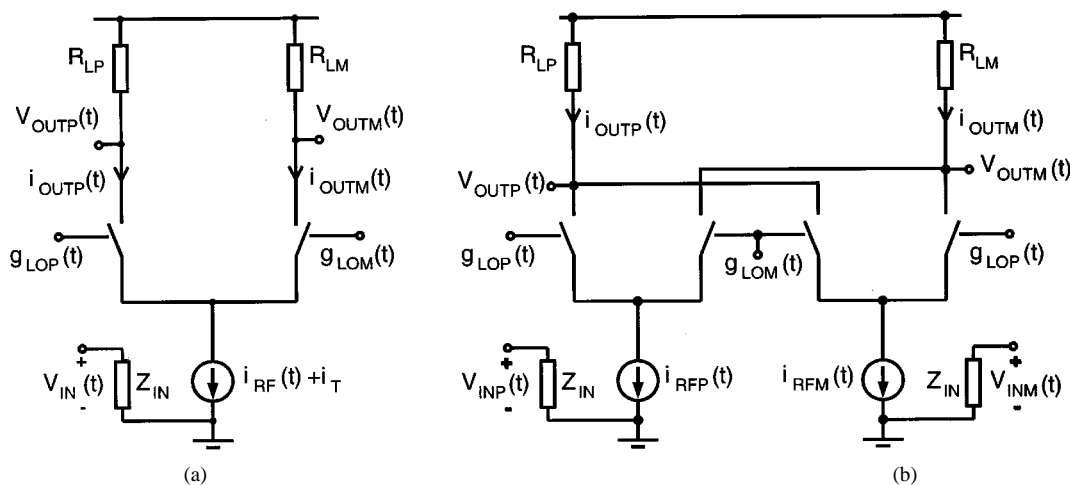


Fig. 2. (a) Behavioral model for single-balanced switching mixer. (b) Behavioral model for double-balanced switching mixer.

to this component, which defines the fundamental nonlinearity of the mixer. In the analysis, the nonlinear VCCS is given as

$$i_{RF}(t) = g_m [v_{in}(t) + \alpha'_2 v_{in}^2(t) + \alpha'_3 v_{in}^3(t) + \dots]. \quad (1)$$

The relative second-order nonlinear coefficient  $\alpha'_2$  can be predicted with the same accuracy as odd-order nonlinearities by the simulations from a single-ended output. It can be considered as a fundamental level of the second-order nonlinearity for each mixer topology. This gives an estimate of the sensitivity of the circuit to mismatches and, hence, the IIP2. The following analysis is based on the mismatched conditions in balanced mixers. It will be shown that the circuit can exhibit a very good IIP2 even under imbalanced conditions if the natural imbalance of the circuit is compensated by a properly controlled intentionally added imbalance. Throughout the paper, the asymmetry due to imbalance between load resistors has been used to detect the IIP2 and to illustrate the effects of mismatching.

#### A. Single-Balanced Behavioral Model

In the first-order behavioral model, a hard-switching local oscillator (LO) is used. However, the effect of the switching core using linear devices is not negligible in the overall performance. The LO is modeled using a square-wave approximation, in which the duty cycle is used as a mismatch variable,

thus, taking the unequal switch conduction times into account. Hence the dc leakage through the mixer and the asymmetries in the switching operations are included. The Taylor series for LO signals are given separately for positive and negative gate functions as

$$\begin{aligned} g_{LOP}(t) &= \eta_P - \left(\frac{2}{\pi}\right) \left[ \sin(\eta_P \pi) \cos(\omega_{LO} t) \right. \\ &\quad - \frac{1}{2} \sin(2\eta_P \pi) \cos(2\omega_{LO} t) \\ &\quad \left. + \frac{1}{3} \sin(3\eta_P \pi) \cos(3\omega_{LO} t) - \dots \right] \\ g_{LOM}(t) &= \eta_M + \left(\frac{2}{\pi}\right) \left[ \sin((1 - \eta_M) \pi) \cos(\omega_{LO} t) \right. \\ &\quad - \frac{1}{2} \sin(2(1 - \eta_M) \pi) \cos(2\omega_{LO} t) \\ &\quad \left. + \frac{1}{3} \sin(3(1 - \eta_M) \pi) \cos(3\omega_{LO} t) - \dots \right]. \quad (2) \end{aligned}$$

The different duty cycles of the positive and negative gate functions are modeled by unequal conduction times  $\eta_P = \eta_{nom}(1 + \Delta\eta/2)$  and  $\eta_M = \eta_{nom}(1 - \Delta\eta/2)$ , respectively. Here,  $\eta_{nom}$  is the nominal value of the duty cycle in a single switch (typically 50%), and  $\Delta\eta$  is the mismatch in the duty cycles between the

positive and negative gate functions. In this analysis, the interest is in the downconversion of the fundamental signal defining the gain and in the even-order nonlinear components around the dc at the output. The currents in the positive and negative branches can be calculated for the terms of interest from

$$\begin{aligned} i_{\text{OUTP}}(t) &= i_{\text{RF}}(t) \cdot g_{\text{LOP}}(t) \\ i_{\text{OUTM}}(t) &= i_{\text{RF}}(t) \cdot g_{\text{LOM}}(t). \end{aligned} \quad (3)$$

The RF input signal of a two-tone test is given as  $A_{\text{RF}}[\cos(\omega_{\text{RF1}}t) + \cos(\omega_{\text{RF2}}t)]$ , and, thus, by substituting (1) and (2) into (3) the low-pass filtered output currents can be given as

$$\begin{aligned} i_{\text{OUTP,LPF}}(t) &= -\frac{1}{\pi} \sin(\eta_P \pi) g_m A_{\text{RF}} \cos(\omega_{\text{IF}} t) \\ &\quad + \eta_P I_T + \eta_P g_m \alpha_2' A_{\text{RF}}^2 [1 + \cos(\omega_{\text{imd2}} t)] \\ i_{\text{OUTM,LPF}}(t) &= \frac{1}{\pi} \sin((1 - \eta_M) \pi) g_m A_{\text{RF}} \cos(\omega_{\text{IF}} t) \\ &\quad + \eta_M I_T + \eta_M g_m \alpha_2' A_{\text{RF}}^2 [1 + \cos(\omega_{\text{imd2}} t)]. \end{aligned} \quad (4)$$

Here,  $\omega_{\text{IF}} = \omega_{\text{RF1}} - \omega_{\text{LO}}$  is the downconverted signal and  $\omega_{\text{imd2}} = \omega_{\text{RF1}} - \omega_{\text{RF2}}$  is the low-frequency beat. The differential output voltage of interest in Fig. 2(a) is

$$\begin{aligned} v_{\text{OUT}}(t) &= v_{\text{OUTP}}(t) - v_{\text{OUTM}}(t) \\ &= i_{\text{OUTP,LPF}}(t) \cdot R_{\text{LP}} - i_{\text{OUTM,LPF}}(t) \cdot R_{\text{LM}} \end{aligned} \quad (5)$$

where  $R_{\text{LP}}$  and  $R_{\text{LM}}$  are the positive and negative load resistances, respectively. The second mismatch term, in addition to an unequal duty cycle, is the imbalance in the load devices. The load resistors are given as  $R_{\text{LP}} = R_L(1 + \Delta R/2)$  and  $R_{\text{LM}} = R_L(1 - \Delta R/2)$ . Here,  $R_L$  is the nominal value of the load resistance and  $\Delta R$  the deviation from the nominal. Hence,  $v_{\text{OUT}}(t)$  becomes

$$\begin{aligned} v_{\text{OUT}}(t) &= -\frac{2}{\pi} g_m R_L A_{\text{RF}} \cos(\omega_{\text{IF}} t) \\ &\quad \cdot \left[ \sin(\eta_{\text{nom}} \pi) \cos\left(\frac{\Delta \eta \cdot \eta_{\text{nom}} \pi}{2}\right) \right. \\ &\quad \left. + \frac{\Delta R}{4} \cos(\eta_{\text{nom}} \pi) \sin\left(\frac{\Delta \eta \cdot \eta_{\text{nom}} \pi}{2}\right) \right] \\ &\quad + \eta_{\text{nom}} [I_T + g_m \alpha_2' A_{\text{RF}}^2 [1 + \cos(\omega_{\text{imd2}} t)]] \\ &\quad \cdot R_L \cdot (\Delta \eta + \Delta R). \end{aligned} \quad (6)$$

The voltage gain can be expressed as

$$A_V = \frac{2}{\pi} g_m R_L \cdot \cos\left(\frac{\Delta \eta \cdot \eta_{\text{nom}} \pi}{2}\right). \quad (7)$$

The cosine term is close to unity, with small  $\Delta \eta$  and, hence, the gain simplifies to the well-known  $(2/\pi)g_m R_L$  formula being almost independent of mismatches, but degrades to some extent when both commutating switches are simultaneously ON or OFF.

The second-order input intercept point is now calculated from the fundamental and the *imd2* terms in (6) as

$$\begin{aligned} \text{iip2} &= \left| \frac{\alpha_1}{\alpha_2} \right| = \frac{2 \sin(\eta_{\text{nom}} \pi) \cos\left(\frac{\Delta \eta \cdot \eta_{\text{nom}} \pi}{2}\right)}{\pi \eta_{\text{nom}} \alpha_2' |\Delta \eta + \Delta R|} \\ &\approx \frac{2}{\pi \eta_{\text{nom}} \alpha_2' |\Delta \eta + \Delta R|}. \end{aligned} \quad (8)$$

The value is an rms-voltage quantity. It is practical to refer the values to the 50- $\Omega$  input power, i.e., IIP2 [dBm] =  $10 \log(1000(\text{iip2})^2/50)$ . According to (8), iip2 depends both on the fundamental second-order distortion,  $\alpha_2'$ , and on the mismatch terms  $\Delta \eta$  and  $\Delta R$ . The former can be defined from the single-ended output of the mixer. It is not directly the  $\alpha_1/\alpha_2$  ratio of the transconductance element because of the switching function. The single-ended iip2 defined either from the positive or negative output is

$$\text{iip2}_{\text{SE}} = \frac{1}{\pi \eta_{\text{nom}} \alpha_2'}. \quad (9)$$

This term is independent of the balancing and can be simulated with the same reliability as odd-order parameters like IIP3. A larger value always indicates reduced sensitivity against envelope distortion. Also, a direct measurement is possible. A similar approach can be used for a double-balanced configuration by applying only a single-ended signal to the RF input. To alleviate the necessity of excellent balancing, a quantity of balancing factor is defined here as

$$D_{\text{BAL}} = \frac{2}{|\Delta \eta + \Delta R|}. \quad (10)$$

The balancing factor depends on the matching properties of the devices in the IC process and the layout of the circuit. If the probability distribution functions of the different process parameters are known, and the sources of mismatches are recognized in the circuit topology, then the balancing factor can be used to estimate the yield of certain IIP2 value. Another important parameter in the direct conversion mixer is the dc offset at the output, which follows from (6) as

$$V_{\text{DC}} = \eta_{\text{nom}} R_L (I_T + g_m \alpha_2' A_{\text{RF}}^2) \cdot (\Delta \eta + \Delta R). \quad (11)$$

The dc term depends also on the amplitude modulation component as given in [2]. IIP2 is plotted as a function of load resistor imbalance with the different  $\alpha_2'$ -parameters in Fig. 3(a). The mismatch in the load is a significant reason for the IIP2 degradation, but the fundamental nonlinearity is also very important for the performance. The selected  $\alpha_2'$ -values (1.8, 0.57, 0.285, 0.1425) correspond to the mixer IIP2-values of 50, 60, 66, and 72 dBm's in the presence of 1% resistor mismatch. The single-ended IIP2 is +20 dBm as  $\alpha_2'$  is 0.285, which is considered as a nominal value throughout the paper. In Fig. 3(b), both the load resistor and switch conduction time imbalances are included simultaneously. The figure shows that two imbalances may degrade the performance significantly from a single mismatch if they are summed. On the other hand, the IIP2 maximum shifts as a function of the other mismatch, as could be expected.

### B. Double-Balanced Behavioral Model

For double-balanced mixers, the transconductance mismatch of the V-I converter and the amplitude and phase imbalances of the RF input signal are added to the analysis. The behavioral model of a double-balanced mixer is shown Fig. 2(b) and can be analyzed in a similar way to the single-balanced topology. Now the V-I converters in each branch are independent voltage-controlled current sources instead of a differential pair. Hence, there is no common-mode rejection in the input stage and it is assumed in the analysis that the tail current is divided equally between the devices. The positive and negative input signals are given separately as

$$\begin{aligned} v_{\text{INP}}(t) &= \frac{A_{\text{RFP}}}{\sqrt{2}} [\cos(\omega_{\text{RF1}}t) + \cos(\omega_{\text{RF2}}t)] \\ v_{\text{INM}}(t) &= -\frac{A_{\text{RFM}}}{\sqrt{2}} [\cos(\omega_{\text{RF1}}t + \Delta\varphi) + \cos(\omega_{\text{RF2}}t + \Delta\varphi)] \end{aligned} \quad (12)$$

where  $\Delta\varphi$  is the phase imbalance between the differential inputs. The amplitudes at the inputs are  $A_{\text{RFP}} = A_{\text{RF}}(1 + \Delta A_{\text{RF}}/2)$  and  $A_{\text{RFM}} = A_{\text{RF}}(1 - \Delta A_{\text{RF}}/2)$  for the positive and negative inputs, respectively. Here,  $\Delta A_{\text{RF}}$  is the amplitude imbalance. The total transconductance of the V-I converter is set to be equal as in the single-balanced mixer analysis, and hence, the  $g_m$  of the input devices can be given as  $g_{mP} = g_m(1 + \Delta g_m)/2$  and  $g_{mM} = g_m(1 - \Delta g_m)/2$  for positive and negative transconductances, respectively. The non-linearity factors,  $\alpha'_n$ , are assumed equal in both input branches. If a comparison between the single- and double-balanced mixers is made, the given assumptions should be characterized separately with respect to biasing and other transistor level parameters. However, they are sufficient when the theoretical differences in the IIP2 behavior are analyzed.

Based on the detailed analysis given in Appendix A, the IIP2 for double-balanced topology can now be written as

$$\begin{aligned} \text{iip2} \approx & \frac{\sqrt{2}}{\pi\eta_{\text{mom}}\alpha'_2} \\ & \cdot \frac{4}{(2\Delta\eta(\Delta g_m + \Delta A_{\text{RF}}) + \Delta R(1 + \Delta g_m)(1 + \Delta A_{\text{RF}}))}. \end{aligned} \quad (13)$$

The IIP2 of a double-balanced mixer is very sensitive to the mismatch in the load resistors according to (13). It is not as sensitive to the errors in the duty cycle because of the double-balanced configuration. The transconductance and input amplitude mismatches have an equal effect on IIP2. Fig. 4(a) illustrates the IIP2 of the single- and double-balanced mixers as a function of the sole load resistor imbalance. The better performance of the double-balanced mixer is due to its smaller gain in this analysis. The phase imbalance at the input of the mixer can be considered negligible according to the analysis. In the presence of several mismatches in the circuit, an excellent load resistor match becomes crucial. Even a small imbalance in the load shifts the maximum of IIP2 far from its original location as shown in Fig. 4(b). The curves plotted for fixed  $\Delta R$  values show that even a 0.1% mismatch can strongly degrade the IIP2, and a 0.5%

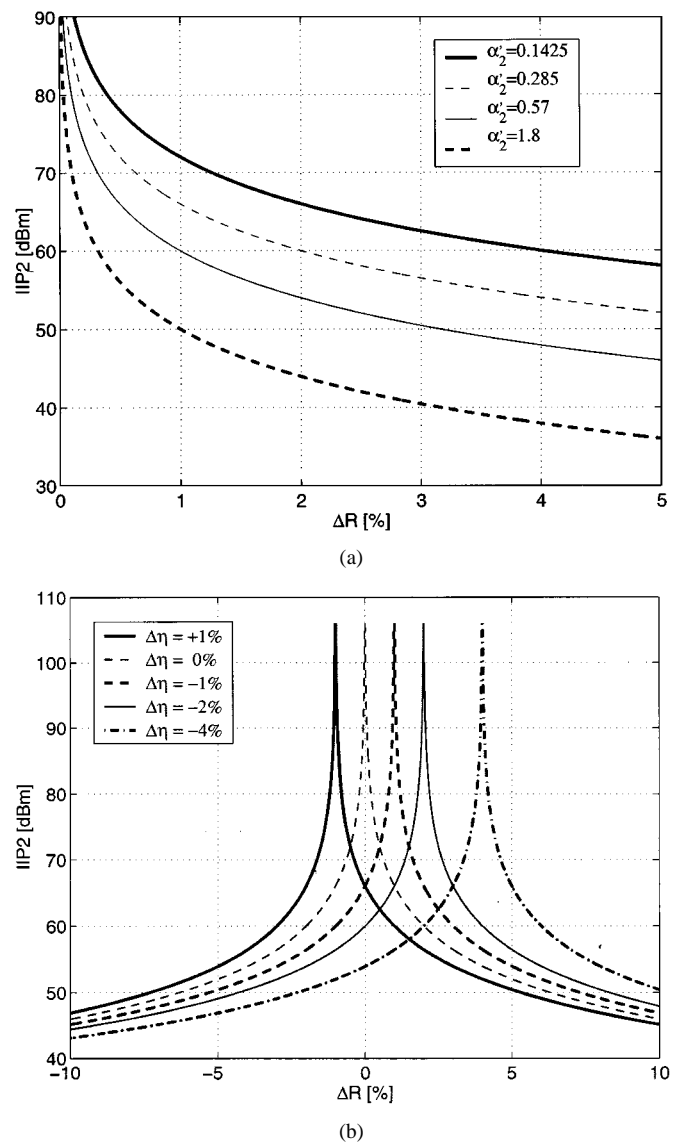


Fig. 3. (a) Calculated effect of nonlinearity parameter  $\alpha'_2$  on IIP2 as a function of load resistor imbalance. (b) Calculated IIP2 as a function of  $\Delta R$  for different  $\Delta\eta$  values.

mismatch is not acceptable. This is because of summation of  $\Delta R$  with multiplied  $\Delta A_{\text{RF}}$  and  $\Delta\eta$  in (13). Input amplitude and transconductance mismatches are in the same role in (13) and, therefore,  $\Delta g_m$  is kept zero in Fig. 4(b).

According to analysis in Appendix A, the dc offset in a double-balanced mixer is

$$V_{\text{DC}} = R_L \cdot \eta_{\text{mom}} \cdot \frac{\Delta R}{2} \left( 2I_T + \frac{1}{2}g_m \cdot \alpha'_2 \cdot A_{\text{RF}}^2 \right). \quad (14)$$

By comparing this to (13), it is obvious that the maximum IIP2 is not necessarily achieved when the dc offset is zero because of the different mismatch terms effective in these two equations.

### C. IIP2 Single-Balanced Behavioral Model Using Bipolar Core

In the previous analysis, the properties of the mixer core transistors were neglected; in this section, a bipolar switching pair replaces the ideal switches in the core. The first-order large

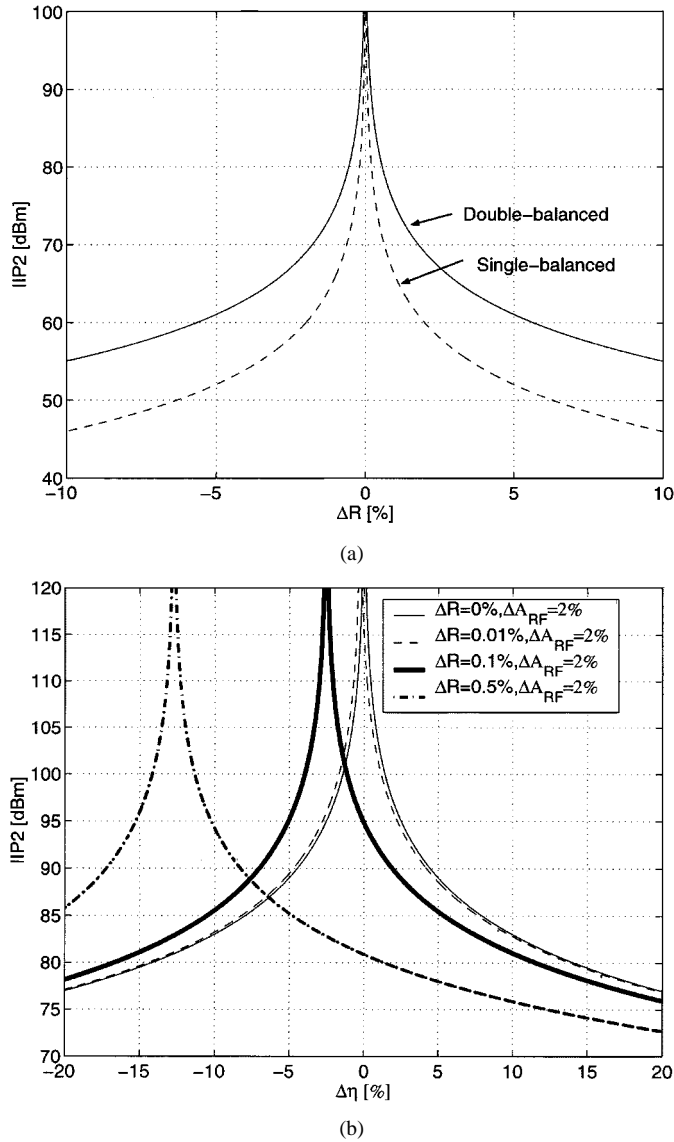


Fig. 4. (a) IIP2 as a function of  $\Delta R$  for single- and double-balanced mixers. (b) IIP2 for double-balanced mixer as a function of  $\Delta \eta$  in the presence of other imbalances.

signal model for the collector current of a bipolar transistor operating as a switch in the core can be given as

$$I_C = I_S e^{\frac{v_{bc}}{V_t}} = I_S e^{\frac{V_{BE} + v_{LO}(t)/2}{V_t}} = I_0 e^{\frac{v_{LO}(t)}{2V_t}} \quad (15)$$

where  $I_S$  is the device saturation current,  $V_t = kT/q$ ,  $V_{BE}$  is the base-emitter bias voltage,  $v_{LO}(t)$  is the differential LO voltage in the switching pair, and  $I_0 = I_S \exp(V_{BE}/V_t)$ . The transfer function of the switching pair then follows the well-known  $\tanh(v_{LO}/2V_t)$  behavior [15]. When the LO voltage is sufficiently large, the mixer conversion gain becomes directly from the ideal brick wall switching function. Otherwise, the amplitude of the LO signal affects the voltage gain given in [16] as

$$\Delta A_V = 20 \log \left( \tanh \left( \frac{A_{LO}}{2V_t} \right) \right) \quad (16)$$

where  $A_{LO}$  is the differential amplitude of the LO signal.

The effect of core transistors on the IIP2 is not negligible in direct conversion receivers and neither is its modeling straight-

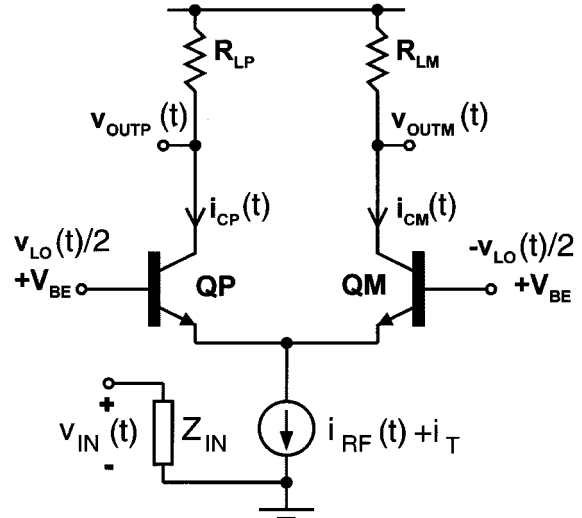


Fig. 5. Single-balanced mixer using a bipolar core.

forward. A large variety of different effects are described in the case of weak nonlinear behavior both for bipolar and MOS devices in [17]. However, the characterization of the switch in the ON state as a cascode stage and in the OFF state as an open circuit is indeed quite inaccurate mainly because many nonidealities in the mixer come from the strongly nonlinear switching operation. Unfortunately the nonlinear characterization of the core leads to complicated equations, which can be solved only numerically [4]. In the case of IIP2, the equations should be combined with the mismatch analysis and the results are assumed not to give more insight as to the nature of the phenomenon than the simplified analysis presented below.

The model in (1) is still used as the only nonlinear function. In addition to the load mismatch, the saturation current mismatch,  $\Delta I_S$ , of the bipolar switching pair is included as another mismatch term. It is in the same role as the duty-cycle mismatch,  $\Delta \eta$ , used earlier, and gives a more realistic model for the core. The analysis in general follows the approach for emitter-coupled pairs given in [15]; some assumptions are made to simplify the mathematics. In all active devices, the output conductances are assumed to be negligible. The emitter resistors of the core transistors are omitted, as the solution in a closed form would be otherwise impossible. Also, the base current is assumed to be much smaller than the collector current. The circuit topology used in the analysis is given in Fig. 5, and (17) and (18) are derived in the Appendix.

The dc offset at the output follows again the same mismatch behavior as the IMD2 component. Only the tail current is added to the RF dependent term as

$$V_{DC} = (I_T + g_m \alpha'_2 R_L A_{RF}^2) \cdot \left[ \Delta R + \frac{\Delta I_S}{2} \cdot \left( 1 - \frac{1}{\frac{3}{2} + \frac{1}{2} \cosh \left( \frac{A_{LO}}{V_t} \right)} \right) \right] \quad (17)$$

The second-order input intercept point becomes

$$iip2 = \frac{2 \tanh \left( \frac{A_{LO}}{2V_t} \right)}{\pi \alpha'_2 \cdot \left| \Delta R + \frac{\Delta I_S}{2} \cdot \left( 1 - \frac{1}{\frac{3}{2} + \frac{1}{2} \cosh \left( \frac{A_{LO}}{V_t} \right)} \right) \right|} \quad (18)$$

TABLE I  
IMBALANCES IN THE CURVES OF FIG. 6

Curve no:	1	2	3	4	5	6	7	8
$\Delta R / \%$	+1	+1	+1	0	0	+1	+1	+1
$\Delta I_S / \%$	0	+1	-1	+1	+5	-2	-2.5	-4

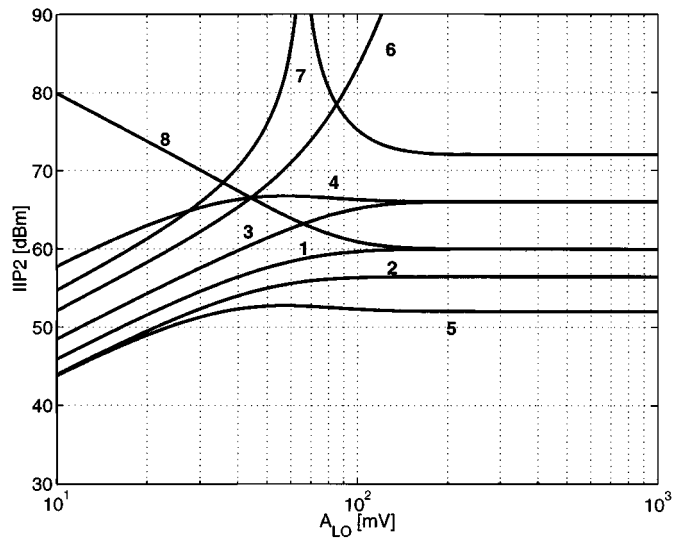


Fig. 6. IIP2 as a function of LO amplitude. Explanations for different IIP2 curves are in the text and in Table I.

The result can now be plotted as a function of the LO amplitude. Several curves according to mismatch conditions given in Table I are shown in Fig. 6. The analysis shows that only a  $\pm 1\%$  variation in  $I_S$  can change IIP2 about 10 dB as the mixer is driven in the switching mode, i.e.,  $A_{LO} > 2V_t$ , as seen from curves 1–3. On the other hand, curves 6–8 indicate that IIP2 can either degrade or improve as a function of LO amplitude, depending on the mismatches. Small peaking as shown in curves 4 and 5 may change to tremendous variations in curves 6–8 when mismatches will cancel each other at certain points. The measured results that will be presented in Section IV show that such variations are also possible in reality. Hence, IIP2 is dependent both on the small mismatches and on the LO amplitude. This simple approach allows practical means to calculate some selected sources of mismatch and an understanding of their relations to IIP2 behavior.

### III. SIMULATIONS

The mixers used in the simulations are single- and double-balanced configurations with a bipolar switching core and MOS input stage, as shown in Fig. 7(a) and (b), respectively. The double-balanced mixer is used earlier in [18] and [19]. Later, this configuration has been used as a platform in the design of more sophisticated downconverters in [20] and [21].

In order to study the contribution of the switching quad in the mixer overall linearity, the nonlinear MOS transconductors can be replaced by a linear voltage-controlled current sources. In the simulations, IIP2 saturates in strongly mismatched conditions to about +25 dBm in the single-balanced mixer, rising only to +36 dBm with a linear equivalent model. In the double-balanced mixer, the corresponding numbers are +30 and +72 dBm,

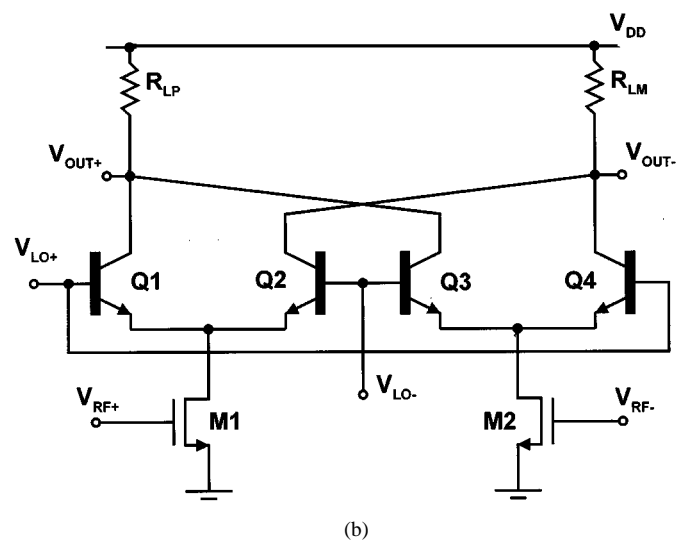
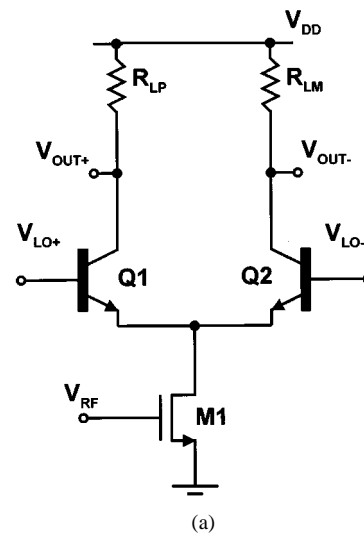


Fig. 7. (a) Single-balanced BiCMOS mixer. (b) Double-balanced BiCMOS mixer.

respectively, (see Figs. 8 and 9). These parameters can be compared to third-order linearity performances. The simulated IIP3 of the single-balanced mixer is +7 dBm and +13 dBm with a linear transconductance stage while the corresponding numbers for the double-balanced mixer are +12 dBm and +17 dBm, respectively. Hence, according to the simulations the single-balanced mixer is more sensitive to the even-order distortion due to the switching stage than the double-balanced mixer; this is quite obvious. However, the  $g_m$  input stage still clearly dominates the overall second-order linearity performance in both topologies. In addition, it turns out that the levels at which IIP2 saturates in the presence of a large significant mismatch equals the simulated single-ended IIP2's, which is as might be expected. That simulated single-ended IIP2s are independent of the mismatch, confirms (9). The simulated single-ended IIP2 is +25.5 dBm and +31.3 dBm for single- and double-balanced mixers, respectively.

IIP2 as a function of the LO signal amplitude has been illustrated in Figs. 10 and 11, for single-balanced and double-balanced topologies, respectively. The behavior resembles some of the calculated curves in Fig. 6. Fig. 8 illustrates the IIP2 as a

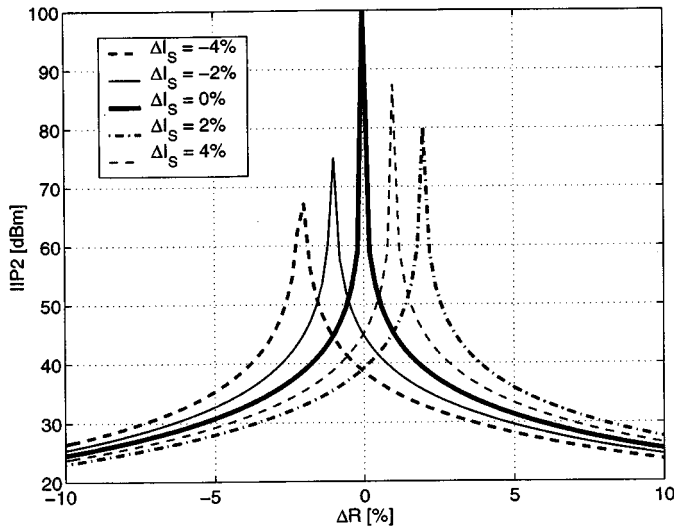


Fig. 8. Simulated IIP2s of single-balanced mixer versus mismatch in load resistors.

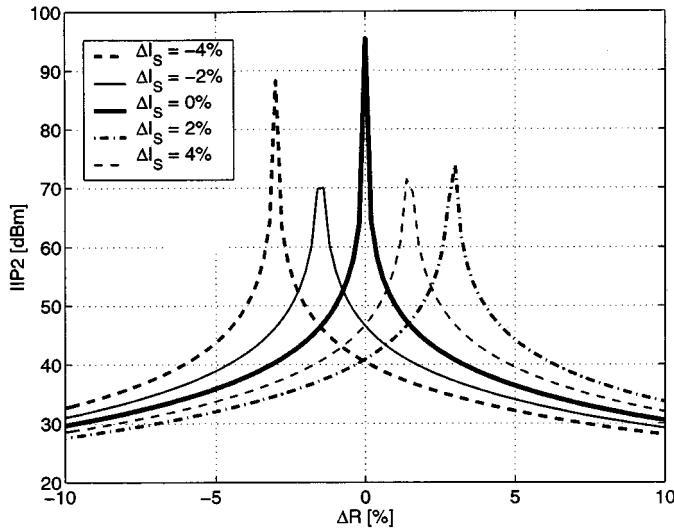


Fig. 9. Simulated IIP2s of double-balanced mixer versus mismatch in load resistors.

function of imbalance in the load resistors with the presence of  $I_S$  imbalance in the switching devices for a single-balanced mixer in the switching mode. As predicted theoretically, the presence of several mismatches shifts the IIP2 maximum. Similar behavior is illustrated for a double-balanced mixer in Fig. 9. However, now the resistor mismatch required to achieve the IIP2 maximum is larger than in the single-balanced case because the maximums are spread wider along the  $\Delta R$ -axis. Nevertheless, at certain IIP2 levels the peaks are wider in the double-balanced case. Hence, a relatively high IIP2 value can be achieved with a larger mismatch.

#### IV. MEASURED RESULTS

The measurements were performed for a single-chip direct conversion receiver [21]. Several circuit samples were measured for the validation of the theoretical calculations and simulations. The receiver is fabricated using a  $0.35\text{-}\mu\text{m}$ ,

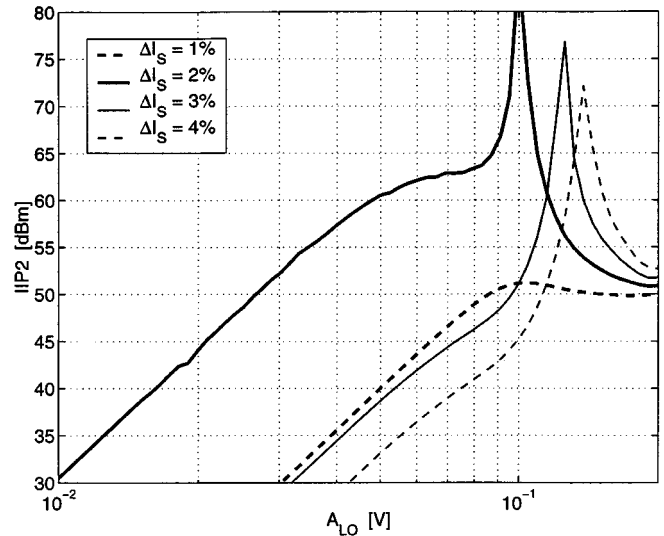


Fig. 10. Simulated IIP2s versus LO amplitude in single-balanced mixer.  $\Delta R = 1\%$ .

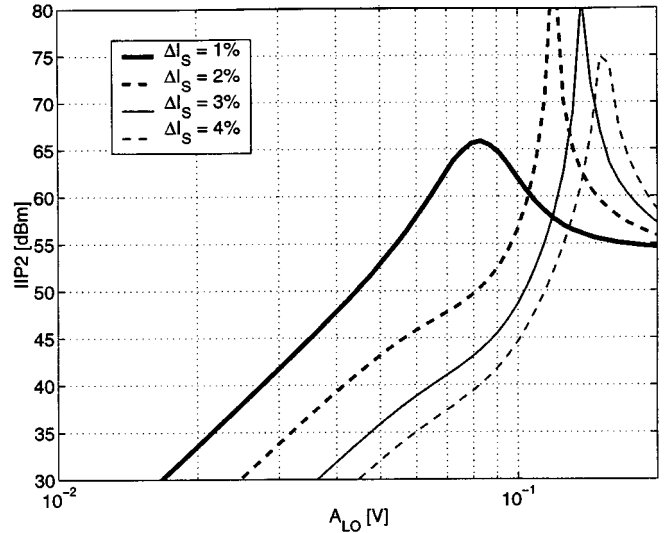


Fig. 11. Simulated IIP2s versus LO amplitude in double-balanced mixer.  $\Delta R = 1\%$ .

SiGe-BiCMOS process, and utilizes a 2.7-V supply. It has interstage I/Os to allow separate measurements for RF and analog baseband circuits. These test I/Os were connected in output terminals of the mixers. The mixer output is unbuffered driving directly the first baseband stage.

The measured mixer output load resistors values match very well in all samples. They were drawn in parallel fingers and dummy structures were used to improve symmetry. The average relative error between the resistor pairs is less than 0.1%. The resistor mismatches and IIP2s are given in Table II. Even though the load resistors match well, significant dc offset exists between the samples. This is an obvious indication that the imbalance is generated elsewhere in the circuit.

The resistive loading allows the insertion of external ac-coupled potentiometers in parallel to load resistors in the test board. Fig. 12 illustrates the trimmed IIP2s versus relative deviation in the load resistances. The given IIP2 is for the mixer, and the gain of the LNA has been extracted from the measured results. The

TABLE II  
MEASURED PERFORMANCE OF SEVERAL SAMPLES

Sample	IIP2(nom) [dBm]	IIP2(trimmed) [dBm]	Improvement [dB]	dc-offset [mV]	$\Delta R$ (nom) [%]
1	41	64	23	-2.8	0.10
2	54	69	15	-3	<0.01
3	54	85	31	-3	0.06
4	41	68	27	11	0.14
5	38	58	20	7	0.24
6	56	84	50	1	0.15

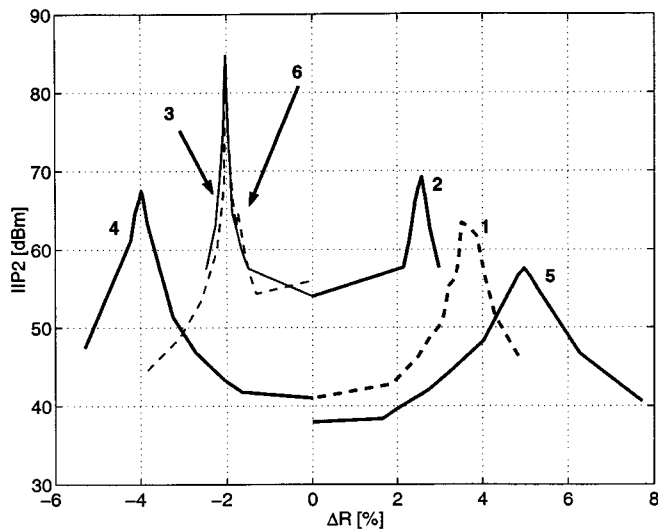


Fig. 12. Trimmed IIP2s of six separate samples. The number of sample is placed next to each curve.

trimmed mixer IIP2 is above +55 dBm in every sample. The improvement in performance is at least 15 dB but the highest benefit is even 50 dB. The numbers are given for each sample in Table II. The dc-offsets remain constant during the tuning due to the ac-coupled potentiometers. However, the IIP2 improvement is achieved in the dc-mismatched conditions, which is earlier shown theoretically. Neither these offsets nor the resistor trimming have a more than negligible effect on the other performance parameters of the measured receiver, e.g., gain, noise figure and IIP3. The direct tuning typically varies the dc offset at the mixer output. However, some amount of dc offset always exists due to natural device mismatching, which has to be removed in direct conversion receiver [22]. The options to remove the offset depend on the system specifications, for example bandwidth and modulation. In some cases, high-pass filtering is a suitable method, which can be implemented by ac-coupling or using a servo feedback loop [23].

The IIP2s were measured also as functions of the LO power. Fig. 13 illustrates IIP2's dependency on LO power for several samples. The IIP2 behaves in a manner similar to that predicted earlier. It can be noticed that there is no observable conformity in the behavior of IIP2 as a function of LO power. However, similar behavior could be expected according to the calculations and simulations. As in Fig. 6, all presented cases appear in the measurements.

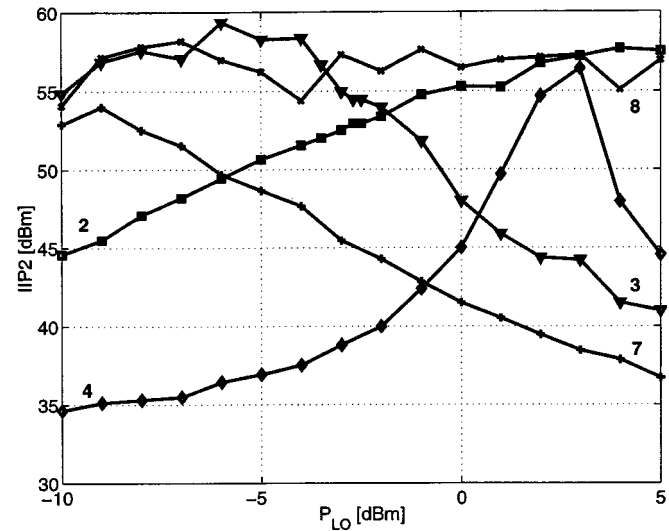


Fig. 13. Measured IIP2 versus LO power. The number of sample is placed next to each curve.

## V. CONCLUSION

A simple theoretical model for envelope distortion behavior in single- and double-balanced mixers has been presented in this paper. The given analysis is more a mismatch analysis than a nonlinearity analysis. It shows clearly why an extensive mismatch analysis is needed to model the IIP2 instead of a complex nonlinearity characterization. This analysis gives a good intuitive sense of the even-order nonlinear behavior of transconductance mixers and is a basis to be extended into other topologies also. The presented theory is consistent with both the simulations and measurements. It has been shown that the linearity maximum can be achieved by the means of even-order distortion in mismatched conditions, even with a presence of a quite significant dc offset. It is evident that this fixed offset can be cancelled by other means in direct conversion receivers. Another important result is that the nonlinearity and imbalance of a circuit can and should be handled separately. The double-balanced topology is not as sensitive to the nonlinearity of the switching core as the single-balanced one. In a single-balanced mixer, the mismatching of the load and the switches have equal effect on the overall linearity. However, the double-balanced topology has slightly different mismatch mechanism compared to the single-balanced mixer. Therefore, the matching of the load resistors becomes even more crucial. With several independent mismatches, the requirements for resistor matching become significantly more stringent than can be estimated when

only resistor mismatch by itself is characterized. This sensitivity to very small parameter variations explains clearly the large dispersion between different samples, which is typical when IIP2 is characterized. On the other hand, the even-order nonlinearity of the double-balanced configuration is undoubtedly dominated by the  $g_m$ -elements and is, thus, less sensitive to the nonlinearity of the switching devices. The elaborate behavior of the IIP2 as a function of LO amplitude is also described theoretically and proved with measurements. However, it again depends on the mismatched conditions only, rather than on the nonlinear characteristics of the core devices.

The presented analysis provides a platform for future developments of mixer linearization by the means of even-order distortion. The theoretical conclusions predict that it may be possible, but difficult, to achieve a high IIP2 even with tuning. However, the simulations and measurements provide more encouraging results. The mismatched conditions can be modeled with a limited number of mismatch parameters although sometimes at least three variables are required. Also, significant improvements in IIP2 can be achieved by tuning only one parameter like the load resistor. It is also important that the odd-order linearity and overall noise performance are not deteriorated as the controlled imbalance has been increased. Nevertheless, the imbalance can slightly affect the increase of common-mode noise detection in mixer output.

#### APPENDIX A

##### DERIVATION OF DOUBLE-BALANCED BEHAVIORAL MODEL

The differential output voltage of a double-balanced topology is

$$v_{\text{OUT}}(t) = [i_{\text{RFP}}(t) \cdot g_{\text{LOP}}(t) + i_{\text{RFM}}(t) \cdot g_{\text{LOM}}(t)] \cdot R_{\text{LP}} - [i_{\text{RFP}}(t) \cdot g_{\text{LOM}}(t) + i_{\text{RFM}}(t) \cdot g_{\text{LOP}}(t)] \cdot R_{\text{LM}}. \quad (\text{A1})$$

When only the desired RF and low frequency terms are considered, the currents of V-I converters can be given as

$$i_{\text{RFP}}(t) = g_{mP} \left[ \frac{A_{\text{RFP}}}{\sqrt{2}} \cos(\omega_{\text{RF1}}t) + \frac{\alpha'_2 A_{\text{RFP}}^2}{2} [1 + \cos(\omega_{\text{imd2}}t)] \right] + \frac{I_T}{2}$$

$$i_{\text{RFM}}(t) = g_{mM} \left[ -\frac{A_{\text{RFM}}}{\sqrt{2}} \cos(\omega_{\text{RF1}}t + \Delta\varphi) + \frac{\alpha'_2 A_{\text{RFM}}^2}{2} [1 + \cos(\omega_{\text{imd2}}t)] \right] + \frac{I_T}{2}. \quad (\text{A2})$$

Assuming that the gate functions of the two pairs of commutating mixers as given in (2) are equal, the low-pass filtered output voltage of the mixer can be given as

$$v_{\text{OUT,LPF}}(t) = -R_L \cdot \left[ a + b - (c + d) + \frac{\Delta R}{2}(a + b + c + d) \right] \quad (\text{A3})$$

where

$$a = \frac{\eta_P}{2} \cdot \left[ I_T - g_{mP} \frac{2 A_{\text{RFP}}}{\pi \sqrt{2}} \cdot \sin(\eta_P \pi) \cdot \cos(\omega_{\text{IF}}t) + g_{mP} \cdot \alpha'_2 \cdot A_{\text{RFP}}^2 (1 + \cos(\omega_{\text{imd2}}t)) \right]$$

$$b = \frac{\eta_M}{2} \cdot \left[ I_T - g_{mM} \frac{2 A_{\text{RFM}}}{\pi \sqrt{2}} \cdot \sin((1 - \eta_M)\pi) \cdot \cos(\omega_{\text{IF}}t) + g_{mM} \cdot \alpha'_2 \cdot A_{\text{RFM}}^2 (1 + \cos(\omega_{\text{imd2}}t)) \right]$$

$$c = \frac{\eta_P}{2} \cdot \left[ I_T + g_{mM} \frac{2 A_{\text{RFM}}}{\pi \sqrt{2}} \cdot \sin(\eta_P \pi) \cdot \cos(\omega_{\text{IF}}t) + g_{mM} \cdot \alpha'_2 \cdot A_{\text{RFM}}^2 (1 + \cos(\omega_{\text{imd2}}t)) \right]$$

$$d = \frac{\eta_M}{2} \cdot \left[ I_T + g_{mP} \frac{2 A_{\text{RFP}}}{\pi \sqrt{2}} \cdot \sin((1 - \eta_M)\pi) \cdot \cos(\omega_{\text{IF}}t) + g_{mP} \cdot \alpha'_2 \cdot A_{\text{RFP}}^2 (1 + \cos(\omega_{\text{imd2}}t)) \right]. \quad (\text{A4})$$

The terms  $a$ ,  $b$ ,  $c$ , and  $d$  present the combinations of positive and negative currents and gate functions multiplied by each other. The voltage gain of a double-balanced mixer is again relatively independent of mismatch and can, thus, be given as

$$A_V = \frac{1}{\sqrt{2}} \cdot \frac{2}{\pi} g_m R_L. \quad (\text{A5})$$

The difference of  $1/\sqrt{2}$  compared to the single-balanced gain in (7), comes from the single-ended to differential conversion at the input. The second-order intermodulation term at the output is

$$A_{\text{imd2}} = \frac{1}{4} R_L A_{\text{RF}}^2 g_m \alpha'_2 \eta_{\text{nom}} \times \left[ 2\Delta\eta \left( \Delta g_m + \Delta A_{\text{RF}} + \Delta g_m \cdot \frac{\Delta A_{\text{RF}}^2}{4} \right) + \Delta R (1 + \Delta g_m) \left( 1 + \Delta A_{\text{RF}} + \frac{\Delta A_{\text{RF}}^2}{4} \right) \right]. \quad (\text{A6})$$

If the squared amplitude mismatches  $\Delta A_{\text{RF}}^2$  are considered insignificant in the summation, IIP2 can be written in the form of (13).

#### APPENDIX B

##### DERIVATION OF SINGLE-BALANCED BEHAVIORAL MODEL USING BIPOLAR CORE

The LO collector currents, in Fig. 5, in each branch are

$$i_{\text{CP}}(t) = I_{0P} e^{\frac{v_{\text{LO}}(t)}{2V_t}} \quad i_{\text{CM}}(t) = I_{0M} e^{-\frac{v_{\text{LO}}(t)}{2V_t}}. \quad (\text{B1})$$

The current ratio between the differential branches can now be written as

$$\frac{i_{\text{CP}}(t)}{i_{\text{CM}}(t)} = \frac{I_{\text{SP}}}{I_{\text{SM}}} \cdot e^{\frac{v_{\text{LO}}(t)}{V_t}}. \quad (\text{B2})$$

The current equation in the emitters of the core transistors is

$$\begin{aligned} i_{\text{RF}}(t) + I_T &= i_{\text{EP}}(t) + i_{\text{EM}}(t) \\ &= \frac{1}{\alpha}(i_{\text{CP}}(t) + i_{\text{CM}}(t)) \approx i_{\text{CP}}(t) + i_{\text{CM}}(t). \end{aligned} \quad (\text{B3})$$

As long as the current gain of the transistor is large,  $\alpha$  is close to unity and the last approximation is valid. Hence, the output voltage becomes

$$\begin{aligned} v_{\text{OUT}}(t) &= v_{\text{OUTP}}(t) - v_{\text{OUTM}}(t) \\ &= i_{\text{CM}}(t) \cdot R_{\text{LM}} - i_{\text{CP}}(t) \cdot R_{\text{LP}} \\ &= [i_{\text{CM}}(t) - i_{\text{CP}}(t)] \cdot R_L \\ &\quad - [i_{\text{CM}}(t) + i_{\text{CP}}(t)] \cdot \Delta R \cdot R_L. \end{aligned} \quad (\text{B4})$$

The saturation currents of core transistors are given as  $I_{\text{SP}} = I_S(1 + \Delta I_S/2)$  and  $I_{\text{SM}} = I_S(1 - \Delta I_S/2)$ . By combining (B2) and (B3) the difference and sum terms in (B4) become

$$\begin{aligned} i_{\text{CM}}(t) - i_{\text{CP}}(t) &= (I_T + i_{\text{RF}}(t)) \\ &\cdot \left[ \tanh\left(\frac{v_{\text{LO}}(t)}{2V_t}\right) + \frac{\Delta I_S}{2} \cdot \left(1 - \frac{1}{1 + \cosh\left(\frac{v_{\text{LO}}(t)}{V_t}\right)}\right) \right] \\ i_{\text{CM}}(t) + i_{\text{CP}}(t) &= (I_T + i_{\text{RF}}(t)) \\ &\cdot \left[ 1 + \frac{\Delta I_S}{2} \cdot \tanh\left(\frac{v_{\text{LO}}(t)}{2V_t}\right) \right]. \end{aligned} \quad (\text{B5})$$

The output voltage can now be written as

$$\begin{aligned} v_{\text{OUT}}(t) &\approx (I_T + i_{\text{RF}}(t)) \cdot R_L \\ &\cdot \left[ \tanh\left(\frac{v_{\text{LO}}(t)}{2V_t}\right) + \Delta R + \frac{\Delta I_S}{2} \right. \\ &\cdot \left. \left(1 - \frac{1}{1 + \cosh\left(\frac{v_{\text{LO}}(t)}{V_t}\right)}\right) \right]. \end{aligned} \quad (\text{B6})$$

The tanh-function presents the transfer function of odd harmonics while the other terms describe the dc leakage and even harmonics in the downconversion. The factor multiplying the current and load resistance is actually the gate function for the bipolar core. However the separation of different frequency components is practically impossible if a sinusoidal LO signal is used in the analysis. The Taylor series expansion for a function in the form of  $\tanh(\alpha \sin(\omega_{\text{LO}}t))$  requires a very large number of terms to find the correct factor for the desired  $\sin(\omega_{\text{LO}}t)$  frequency component if  $\alpha$  is large, i.e., in the case of a switching mixer. However, it is still possible to use the gain degradation function (16) as the approximation of the fundamental downconverted signal. Hence, the amplitude of the IF output is given as

$$A_{\text{IF}} = \frac{2}{\pi} g_m R_L A_{\text{RF}} \tanh\left(\frac{A_{\text{LO}}}{2V_t}\right). \quad (\text{B7})$$

The same problems as above apply also for Taylor series of  $\cosh(\alpha \sin(\omega_{\text{LO}}t))$ . However, the interest here is only in the dc leakage term of the gate function because the nonlinearity comes from the V-I converter. Also, the possible downconversion from the second harmonic of the LO is neglected. Hence, the dc term of the  $\cosh(\alpha \sin(\omega_{\text{LO}}t))$  is given as  $(\cosh(\alpha) + 1)/2$ . The amplitude of the low-frequency imd2 term at the output can now be written as

$$\begin{aligned} A_{\text{imd2}} &= g_m \alpha'^2 R_L A_{\text{RF}}^2 \\ &\cdot \left[ \Delta R + \frac{\Delta I_S}{2} \cdot \left(1 - \frac{1}{\frac{3}{2} + \frac{1}{2} \cosh\left(\frac{A_{\text{LO}}}{V_t}\right)}\right) \right]. \end{aligned} \quad (\text{B8})$$

#### ACKNOWLEDGMENT

The authors would like to thank J. Ryyänen and J. Jussila for their assistance with this paper.

#### REFERENCES

- [1] A. Abidi, "Direct-conversion radio transceivers for digital communications," *IEEE J. Solid-State Circuits*, vol. 30, pp. 1399–1410, Dec. 1995.
- [2] B. Razavi, "Design considerations for direct-conversion receivers," *IEEE Trans. Circuits Syst. II*, vol. 44, pp. 428–435, June 1997.
- [3] E. E. Bautista, B. Bastani, and J. Heck, "A high IIP2 downconversion mixer using dynamic matching," *IEEE J. Solid-State Circuits*, vol. 35, pp. 1934–1941, Dec. 2000.
- [4] R. G. Meyer, "Intermodulation in high-frequency bipolar transistor integrated-circuit mixers," *IEEE J. Solid-State Circuits*, vol. SC-21, pp. 534–537, Aug. 1986.
- [5] M. T. Terrovitis and R. G. Meyer, "Intermodulation distortion in current-commutating CMOS mixers," *IEEE J. Solid-State Circuits*, vol. 35, pp. 1461–1473, Oct. 2000.
- [6] K. L. Fong and R. G. Meyer, "High-frequency nonlinearity analysis of common-emitter and differential-pair transconductance stages," *IEEE J. Solid-State Circuits*, vol. 33, pp. 548–555, Apr. 1998.
- [7] C. D. Hull and R. G. Meyer, "A systematic approach to the analysis of noise in mixers," *IEEE Trans. Circuits Syst. I*, vol. 40, pp. 909–919, Dec. 1993.
- [8] M. T. Terrovitis and R. G. Meyer, "Noise in current-commutating CMOS mixers," *IEEE J. Solid-State Circuits*, vol. 34, pp. 772–783, June 1999.
- [9] H. Darabi and A. Abidi, "Noise in RF-CMOS mixers: A simple physical model," *IEEE J. Solid-State Circuits*, vol. 35, pp. 15–25, Jan. 2000.
- [10] D. Coffing and E. Main, "Effects of offsets on bipolar integrated circuit mixer even order distortion terms," in *Proc. IEEE MTT-S Dig.*, June 2000, pp. 147–150.
- [11] T. Yamaji, H. Tanimoto, and H. Kokatsu, "An I/Q active balanced harmonic mixer with IM2 cancelers and a 45° phase shifter," *IEEE J. Solid-State Circuits*, vol. 33, pp. 2240–2246, Dec. 1998.
- [12] L. Sheng, J. C. Jensen, and L. E. Larson, "A wide bandwidth Si/SiGe HBT direct conversion sub-harmonic mixer/downconverter," *IEEE J. Solid-State Circuits*, vol. 35, pp. 1329–1337, Sept. 2000.
- [13] W. H. Lambert, "Second-order distortion in CATV push-pull amplifiers," *Proc. IEEE*, vol. 58, pp. 1057–1062, July 1970.
- [14] C. Takahashi, R. Fujimoto, S. Arai, T. Itakura, T. Ueno, H. Tsurumi, H. Tanimoto, S. Watanabe, and K. Hirakawa, "A 1.9 GHz Si direct conversion receiver IC for QPSK modulation systems," in *ISSCC Dig. Tech. Papers*, Feb. 1996, pp. 644–649.
- [15] P. R. Gray and R. G. Meyer, *Analysis and Design of Analog Integrated Circuits*, 2nd ed. New York: Wiley, 1984.
- [16] B. Gilbert, "Design considerations of active BJT mixers," in *Low-Power HF Microelectronics; A Unified Approach*, ser. 8, Inst. Elect. Eng. Circuits and Systems, G. A. S. Machado, Ed., London, U.K., 1996, ch. 23, pp. 837–928.
- [17] P. Wambacq and W. Sansen, *Distortion Analysis of Analog Integrated Circuits*. Norwell, MA: Kluwer, 1998.
- [18] A. Pärssinen, J. Jussila, J. Ryyänen, L. Sumanen, and K. Halonen, "A wide-band direct conversion receiver for WCDMA applications," in *ISSCC Dig. Tech. Papers*, Feb. 1999, pp. 220–221.

- [19] A. Pärssinen, J. Jussila, J. Ryyänen, L. Sumanen, K. Kivekäs, and K. Halonen, "A wide-band direct conversion receiver with on-chip A/D converters," in *Symp. VLSI Circuits Dig. Tech. Papers*, June 2000, pp. 32–33.
- [20] J. Ryyänen, K. Kivekäs, J. Jussila, A. Pärssinen, and K. Halonen, "A dual-band RF front-end for WCDMA and GSM applications," in *Proc. Custom Integrated Circuits Conf.*, May 2000, pp. 175–178.
- [21] J. Jussila, J. Ryyänen, K. Kivekäs, L. Sumanen, A. Pärssinen, and K. Halonen, "A 22 mA 3.7 dB NF direct conversion receiver for 3G WCDMA," in *ISSCC Dig. Tech. Papers*, Feb. 2001, pp. 284–285.
- [22] J. K. Cavers and M. W. Liao, "Adaptive compensation for imbalance and offset losses in direct conversion transceivers," *IEEE Trans. Veh. Technol.*, vol. 42, pp. 581–588, Nov. 1993.
- [23] C. D. Hull, J. L. Tham, and R. R. Chu, "A direct-conversion receiver for 900 MHz (ISM band) spread-spectrum digital cordless telephone," *IEEE J. Solid-State Circuits*, vol. 31, pp. 1955–1963, Dec. 1996.



**Kalle Kivekäs** (S'01) was born in Helsinki, Finland, in 1974. He received the M.Sc. and Licentiate in Technology degrees in electrical engineering, in 1999, and 2001, respectively, from Helsinki University of Technology (HUT), Helsinki, Finland, where he is currently working toward the Ph.D. degree.

He is currently also a Research Engineer at HUT. His research interests are in communications systems and RF integrated circuit design for wireless applications.



**Aarno Pärssinen** (S'95–M'01) received the M.Sc., Licentiate in Technology, and Doctor of Science degrees in electrical engineering from Helsinki University of Technology (HUT), Helsinki, Finland, in 1995, 1997, and 2000, respectively.

From 1994 to 2000, he was with the Electronic Circuit Design Laboratory, HUT, where he worked on direct conversion receivers and subsampling mixers for wireless communications. In 1996, he was a Visiting Researcher at the University of California, Santa Barbara. Since 2000, he has been a Senior Research

Engineer at the Nokia Research Center, Helsinki, Finland. His research interests include RF and analog integrated circuit design for wireless communications systems.



**Kari A. I. Halonen** was born in Helsinki, Finland, in 1958. He received the M.Sc. degree in electrical engineering from Helsinki University of Technology (HUT), Helsinki, Finland, in 1982, and the Ph.D. degree in electrical engineering from the Katholieke Universiteit of Leuven, Heverlee, Belgium, in 1987.

From 1982 to 1984, he was an Assistant at HUT, and a Research Assistant at the Technical Research Centre of Finland, Helsinki, Finland. From 1984 to 1987, he was a Research Assistant at the E.S.A.T. Laboratory of the Katholieke Universiteit Leuven, Heverlee, Belgium, on a temporary grant from the Academy of Finland. From 1988 to 1990, he was a Senior Assistant with the Electronic Circuit Design Laboratory, HUT. From 1990 to 1993, he was the Director of the Integrated Circuit Design Unit of the Microelectronics Centre at HUT. From 1992 to 1993, he was on leave of absence from HUT and was an R&D Manager at Fincitec Inc., Helsinki, Finland. From 1993 to 1996, he was an Associate Professor in the Faculty of the Electrical Engineering and Telecommunications, HUT, where, in 1997, he became a Full Professor. He has authored or coauthored about 100 international and national conference and journal publications on analog integrated circuits. He specializes in CMOS and BiCMOS analog integrated circuits, particularly for telecommunication applications.